This version is available at https://strathprints.strath.ac.uk/56830/

EFFECT OF WEB HOLES ON WEB CRIPPLING STRENGTH OF COLD-FORMED STEEL CHANNEL SECTIONS UNDER END-ONE-FLANGE LOADING CONDITION-PART I: TESTS AND FINITE ELEMENT ANALYSIS

Ying Lian[a], Asraf Uzzaman[b], James B.P Lim[a,c,*], Gasser Abdelal[d],

David Nash[b], Ben Young[e]

a SPACE, David Keir Building, Queen's University, Belfast, BT9 5AG, UK

b Department of Mechanical and Aerospace Engineering, The University of Strathclyde, 75 Montrose Street, Glasgow G1 1XJ, UK

c Civil & Environmental Engineering, The University of Auckland, 20 Symonds Street, Auckland, New Zealand

d Department of Mechanical and Aerospace Engineering, Queen's University, Belfast, BT9 5AH, UK

e Department of Civil Engineering, The University of Hong Kong, Pokfulam Road, Hong Kong

Abstract

Web openings could be used in cold-formed steel beam members, such as wall studs or floor joints, to facilitate ease of services in buildings. In this paper and its companion paper, a combination of tests and non-linear finite element analyses is used to investigate the effect of such holes on web crippling under end-one-flange (EOF) loading condition. The present paper includes a testing programme on web crippling of channel section and material tensile coupons, followed by a numerical study, where the models are firstly validated against the performed experiments. The results of 74 web crippling tests are presented, with 22 tests conducted on channel sections without web openings and 52 tests conducted on channel sections with web openings. In the case of the tests with web openings, the hole was either located centred above the bearing plates or having a horizontal clear distance to the near edge of the bearing plates. A non-linear finite element model is described, and the results compared against the laboratory test results; a good agreement between the tests and finite element analyses was obtained in term of both strength and failure modes.

Nomenclature	
A	Web holes ratio;
a	Diameter of circular web holes;
a_{LHS}	Diameter of circular web holes positioned left hand side of specimen;
a_{RHS}	Diameter of circular web holes positioned right hand side of specimen;
b_f	Overall flange width of section;
b_l	Overall lip width of section;
COV	Coefficient of variation;
d	Overall web depth of section;
E	Young's modulus of elasticity;
FEA	Finite element analysis;
f_y	Material yield strength;
h	Depth of flat portion of web;
L	Length of specimen;
N	Length of bearing plate;
P_{EXP}	Experimental ultimate web crippling load per web;
P_{FEA}	Web crippling strength per web predicted from finite element (FEA);
P_m	Mean value of tested-to-predicted load ratio;
r_i	Inside corner radius of section;
t	Thickness of section;
x	Horizontal clear distance of web holes to near edge of bearing plate;
$\sigma_{0.2}$	Static 0.2% proof stress; and
σ_u	Static ultimate tensile strength.

1 Introduction

Cold-formed steel sections are increasingly used in residential and commercial construction as both primary and secondary framing members. Web crippling at points of concentrated load or reaction is well known to be a significant problem, particularly in thin walled beams. To improve the buildability of buildings composed of cold-formed steel channel-sections, openings in the web are often required, for ease of installation of electrical or plumbing services.

Strength reduction factor equations have recently been proposed by Uzzaman et al. [1-4] for the web crippling strength of cold-formed steel channel sections with circular holes in the web under the end-two-flange (ETF) and interior-two-flange (ITF) loading conditions. This paper extends the work of Uzzaman et al. [1-4] to consider the end-one-flange (EOF) loading condition for cold-formed steel channel sections with circular holes in the web.

In the literature, for the EOF loading condition, LaBoube et al. [5] have previously considered the case of a circular hole having a horizontal clear distance to the near edge of the bearing plates, but only for the case where the flanges are fastened to the bearing plates. The strength reduction factor equation proposed by LaBoube et al. [5] was subsequently adopted by the North American Specification (NAS) [6] for cold-formed steel sections. This strength reduction factor equation, however, was limited to thicknesses ranged from 0.83 mm to 1.42 mm. Other work described in the literature include that of Yu and Davis [7] who studied the case of both circular and square web openings located and centred beneath the bearing plates under interior-one-flange loading condition, and Sivakumaran and Zielonka [8] who considered the case of rectangular web openings located and centred beneath the bearing plates under the interior-one-flange loading condition, and Zhou and Young [9] who proposed strength reduction factor

equations for aluminium alloy square sections with circular web openings located and centred beneath the bearing plates under end- and interior-two flange loading conditions. Recent research on web crippling of cold-formed steel channel sections, other than that by Uzzaman et al. [10-13] who again considered only the two-flange loading conditions, has not covered the case of holes.

The present paper and its companion paper [14] describe a comprehensive experimental study, numerical study and design recommendation of cold-formed steel channel sections with circular web holes under end-one-flange loading condition subjected to web crippling. In this study, a combination of tests and non-linear finite element analyses (FEA) are used to investigate the cases of both flanges fastened and flanges unfastened to the bearing plates, of circular web holes located centred above the bearing plates and with a horizontal clear distance to the near edge of the bearing plates, on the web crippling strength of lipped channel sections for the end-one-flange (EOF) loading condition, as shown in Fig. 1. The general purpose finite element analysis (FEA) program ABAQUS [14] was used for the numerical investigation. The finite element model (FEM) included geometric and material non-linearities; the results of the finite element analysis were verified against laboratory test results. Both the failure loads as well as the modes of failure predicted from the finite element analyses were in good agreement with the laboratory test results. Upon validation of the finite element models, a series of parametric studies are carried out; design recommendations are reported in the companion paper [14].

2 Experimental investigation

2.1 Test specimens

Fig. 2 shows details of the cold-formed steel lipped channel sections, with circular web holes, used in the web crippling test programme. As can be seen from Fig. 3 and Fig. 4, each test comprised a pair of channel sections with a load transfer block bolted between them. Washer plates of thickness 6 mm were bolted to the outside of the webs of the channel-sections.

The size of the web holes was varied in order to investigate the effect of the web holes on the web crippling behaviour. Circular holes with a nominal diameter (a) ranging from 55 mm to 179 mm were considered in the experimental investigation. The ratio of the diameter of the holes to the depth of the flat portion of the webs (a/h) was 0.2, 0.4 and 0.6. All test specimens were fabricated with web holes located at the mid-depth of the webs and centred above the bearing plates, with a horizontal clear distance to the near edge of the bearing plates (x), as shown in Fig. 1.

Channel sections without holes were also tested. The test specimens consisted of three different section sizes, having nominal thicknesses ranging from 1.2 mm to 2.0 mm; the nominal depth of the webs and the flange widths ranged from 142 mm to 302 mm. The measured web slenderness (h/t) values of the channel sections ranged from 111.7 to 157.8. The specimen lengths (L) were determined according to the NAS [6]. Generally, the distance between bearing plates was set to be 1.5 times the overall depth of the web (d) rather than 1.5 times the depth of the flat portion of the web (h), the latter being the minimum specified in the specification.

Tables 1 and 2 show the measured test specimen dimensions for the flanges unfastened and fastened to the bearing plates, respectively, using the nomenclature defined in Figs. 2 and 3 for the EOF loading condition. The bearing plates were fabricated

using high strength steel having a nominal yield strength of 560 MPa and a thickness of 25 mm. Three lengths of bearing plates (N) were used: 100 mm, 120 mm and 150 mm.

2.2 Specimens labelling

In Table 1 and Table 2, the specimens were labelled such that the nominal dimension of the specimen and the length of the bearing plates, as well as the ratio of the diameter of the holes to the depth of the flat portion of the webs (a/h), could be identified from the label. For example, the labels "202x65x15-t1.4-N100-A0-FR-T1" and "202x65x15-t1.4-N100-A0-FX" are explained as follows:

- The first four notations define the nominal dimensions ($d \times b_f \times b_l$–t1.4) of the specimens in millimetres (i.e. $202 \times 65 \times 15$-t1.4 means $d = 202$ mm; $b_f = 65$ mm; $b_l = 15$ mm and $t = 1.4$ mm).

- "N100" represents the length of bearing in millimetres (i.e. 100 mm).

- "A0.2", "A0.4", and "A0.6" represent the ratios of the diameter of the holes to the depth of the flat portion of the webs (a/h) i.e. A0.2 means $a/h = 0.2$; A0.6 means $a/h = 0.6$. In all cases, the holes are located at the mid-depth of the web and with a horizontal clear distance to the near edge of the bearing plate ($x = 0.2h$). Twenty two tests were conducted on the channel section specimens without web holes, and these are denoted by "A0".

- "MA0.3", "MA0.4" and "MA0.6", the letter "M" indicate web holes located at the mid-depth of the webs and centred above the bearing plates.

- "FR" represents flanges unfastened to the bearing plates and "FX" represents flanges fastened to the bearing plates.

- If a test was repeated, then "T1" indicates the first test, "T2" indicates the second test and "T3" indicates the third test.

2.3 Material properties

Tensile coupon tests were carried out to determine the material properties of the channel sections. The tensile coupons were taken from the centre of the web plate in the longitudinal direction of the untested specimens. The tensile coupons were prepared and tested according to the British Standard for tensile testing of metallic materials [16]. The coupons were tested in a MTS displacement controlled testing machine using friction grips. Two strain gauges and a calibrated extensometer of 50 mm gauge length were used to measure the longitudinal strain. The material properties obtained from the tensile coupon tests are summarised in Table 3, which includes the measured static 0.2% proof stress ($\sigma_{0.2}$) and the static tensile strength (σ_u) based on gauge length of 50 mm.

2.4 Test rig and procedure

The specimens were tested under the end-one-flange (EOF) loading condition specified in the NAS [6], as shown in Fig. 3(a), Fig. 3(b), Fig. 4(a), Fig. 5(a), Fig. 6(a) and Fig. 7(a), where two channel specimens were used to provide symmetric loading. The specimens were bolted to a load transfer block at the central loading point. Two identical bearing plates of the same width were positioned at both ends of the specimen. Hinge supports were simulated by two half rounds in the line of action of the force and teflon pads. Four displacement transducers (LVDTs) were used to measure the vertical displacements. In addition, transducers were located on the flange near the corners for all specimens. A servo-controlled hydraulic testing machine was used to apply a concentrated compressive force to the test specimens. Displacement control was used to drive the hydraulic actuator at a constant speed of 0.05 mm/min. The load was applied through the load transfer plate bolted to the channel sections. All the bearing plates were fabricated using high strength steel having a nominal yield stress of 560 MPa, and thickness of 25 mm. In the experimental investigation, three different lengths of bearing

plates (*N*) were used, namely, 100 mm, 120 mm and 150 mm. The experimental investigation also considered flanges of the channel section specimens fastened or unfastened to the bearing plates, as shown in Fig. 3(c) and Fig. 3(d). For the case of the flanges fastened test set-up, the flanges were bolted to the bearing plates.

2.5 Test results

A total of 74 specimens were tested under the end-one-flange (EOF) loading condition. The experimental ultimate web crippling loads per web (P_{EXP}) are given in Tables 1 and Table 2 for the flanges unfastened and fastened cases, respectively. In order to demonstrate the reliability of the test results, three different channel sections were repeated three times for both flanges unfastened and flanges fastened case; the specimens are 142×60×13-t1.3-N100-A0, 142×60×13-t1.3-N100-A0.4 and 142×60×13-t1.3-N100-MA0.4. The tests results for the repeated tests are very close to their first test values. Fig. 8 and Fig. 9 show the typical failure mode of web crippling of the specimens with web holes and without web holes for the flanges unfastened and fastened, respectively. Typical load-deflection curves obtained from the specimens 142×60×13-t1.3-N100, both without and with web holes are shown in Fig. 10 and Fig. 11.

3 Numerical investigation

3.1 General

The non-linear general purpose finite element program ABAQUS [15] was used to simulate the web crippling behaviour of the channel sections. The bearing plates, the load transfer block, the channel sections and the contact between the bearing plates and the channel section and load transfer block were modelled. The measured cross-section dimensions and the material properties from the tests were used. The channel sections of the model were based on the centreline dimensions of the cross-section. Specific modelling issues are described below.

3.2 Geometry and material properties

Half of the test set-up was modelled, as shown in Fig. 4(b), Fig. 5(b), Fig. 6(b) and Fig. 7(b). The dimensions of the channel section modelled are given in Table 1 and Table 2. Contact surfaces are defined between the bearing plate and the cold-formed steel section. In addition, contact surfaces are defined between the load transfer block and cold-formed steel section.

The value of Young's modulus was 205 kN/mm^2 and Poisson's ratio was 0.3. ABAQUS required the material stress-strain curve input as true stress-true plastic strain. The stress-strain curves were directly obtained from the tensile tests and converted into true stress- true plastic strain curves using Equation 1 and Equation 2, as specified in the ABAQUS manual (2013) [15],

$$\sigma_{true} = \sigma(1+\varepsilon) \qquad\qquad (1)$$

$$\varepsilon_{true(pl)} = \ln(1+\varepsilon) - \frac{\sigma_{true}}{E} \qquad\qquad (2)$$

where E is the Young's Modulus, σ and ε are the engineering stress and strain respectively in ABAQUS [14].

3.3 Element type and mesh sensitivity

Fig. 4(b), Fig. 5(b), Fig. 6(b) and Fig. 7(b) show details of a typical finite element mesh of the channel section, the bearing plate and load transfer block. A mesh sensitivity analysis was used to investigate the effect of different element sizes in the cross-section of the channel sections. Finite element mesh sizes were 5 mm × 5 mm for the cold-formed steel channel sections and 8 mm × 8 mm for the bearing plates and load transfer block.

From the mesh sensitivity analysis, due to the contact between the load transfer block and inside round corners that form the bend between the flange and web, it was found that at least fifteen elements were required for the corners between the flange and

web. On the other hand, for the corners between the flange and lip of the section, only three elements were required.

Cold-formed steel channel sections with and without web holes were modelled using S4R shell element. The S4R is a four-node double curved thin or thick shell element with reduced integration and finite membrane strains. It is mentioned in the ABAQUS Manual [15] that the S4R element is suitable for complex buckling behaviour. The S4R has six degrees of freedom per node and provides accurate solutions to most applications. The bearing plates and load transfer block were modelled using analytical rigid plates and C3D8R element, which is suitable for three-dimensional modelling of structures with plasticity, stress stiffening, large deflection, and large strain capabilities. The solid element is defined by eight nodes having three translational degrees of freedom at each node.

3.4 Loading and boundary conditions

The vertical load applied to the channel sections through the load transfer block in the laboratory tests was modelled using displacement control. In the finite element model, a displacement in the vertical y direction was applied to the nodes located on the top of the load transfer block. The channel section specimens were tested in pairs, which were bolted to a load transfer block at the central loading point through the web by a vertical row of M16 high tensile bolts.

In the shell element idealisation, cartesian connectors were used to simulate the bolts instead of physically modelling bolts and holes. "CONN3D2" connector elements were used to model the in-plane translational stiffness i.e. y- and z-directions. The stiffness of the connectors element was 10 kN/mm, which Lim and Nethercot [17-18] suggest would be suitable. In the x direction, the nodes were prevented from translating.

Contact between the bearing plate and the cold-formed steel section was modelled in ABAQUS using the contact pairs option. The two contact surfaces were not allowed to

10

penetrate each other. No friction was modelled between the surfaces. In the flanges fastened case, in addition to the contact modelled between the bearing plate and the cold-formed steel-sections, a connector between the flanges and the bearing plate was modelled at the position of the bolt.

3.5 Verification of finite element model

A comparison between the experimental results and the finite element results was carried out in order to verify and check the accuracy of the finite element model. The comparison of the web crippling strength per web obtained from the tests (P_{EXP}) and the finite element analysis (P_{FEA}) is shown in Table 4 and Table 5. The comparison of the load-deflection curves for the specimens 142×60×13-t1.3-N100, without and with web holes, are shown in Fig. 10 and Fig 11, respectively. It is observed that good agreement has been achieved for both without web holes and with web holes cases.

For the flanges unfastened to the bearing plates case, the mean value of the ratio P_{EXP}/P_{FEA} is 0.97; the corresponding coefficient of variation (COV) is 0.057. For the flanges fastened to the bearing plates case, the mean value of the ratio P_{EXP}/P_{FEA} is 0.99; the corresponding coefficient of variation (COV) is 0.025.

The web crippling failure mode observed from the tests has been also verified by the finite element model for the EOF loading conditions, as shown in Fig. 4 to Fig. 9. It is shown that good agreement is achieved between the experimental and finite element results for both the web crippling strength and the failure mode.

4 Conclusions

Experimental and numerical investigations on the web crippling behaviour of cold-formed steel lipped channel sections, with and without circular web holes, under the end-one-flange (EOF) loading condition have been presented. A test programme on lipped channel sections with web holes located at the mid-depth of the web and centred above

the bearing plates or with a horizontal clear distance to the near edge of bearing plates were considered. The channel section specimens had measured 0.2% proof stress (yield stresses) of 457 MPa, 464 MPa and 479 MPa for the three different section sizes. The web slenderness values ranged from 111.7 to 157.8. The diameter of the web hole was varied in order to investigate the influence of the web holes on the web crippling behaviour. Flanges of the lipped channel sections were either fastened or unfastened to the bearing plates.

Finite element models have been developed and verified against the experimental results in term of web crippling failure loads and deformations. The finite element models provide a good prediction for the web crippling strength of cold-formed lipped channel sections with and without circular web holes. The verified finite element models are used to carry out an extended study for developing reliable design recommendations for cold-formed steel sections with web holes in the companion paper [14].

References

[1] A. Uzzaman, J.B.P. Lim, D. Nash, J. Rhodes, B. Young, Web crippling behaviour of cold-formed steel channel sections with offset web holes subjected to interior-two-flange loading, Thin-Walled Structures, 50 (2012) 76-86.

[2] A. Uzzaman, J.B.P. Lim, D. Nash, J. Rhodes, B. Young, Effect of offset web holes on web crippling strength of cold-formed steel channel sections under end-two-flange loading condition, Thin-Walled Structures, 65 (2013) 34-48.

[3] A. Uzzaman, J.B.P. Lim, D. Nash, J. Rhodes, B. Young, Cold-formed steel sections with web openings subjected to web crippling under two-flange loading conditions-part I: Tests and finite element analysis, Thin-Walled Structures, 56 (2012) 38-48.

[4] A. Uzzaman, J.B.P. Lim, D. Nash, J. Rhodes, B. Young, Cold-formed steel sections with web openings subjected to web crippling under two-flange loading conditions-part II: Parametric study and proposed design equations, Thin-Walled Structures, 56 (2012) 79-87.

[5] R.A. LaBoube, W.W. Yu, S.U. Deshmukh, C.A. Uphoff, Crippling capacity of web elements with openings, Journal of Structural Engineering, 125 (1999) 137-141.

[6] NAS, North American specification for the design of cold-formed steel structural members, American Iron and Steel Institute, AISI S100-2007, AISI Standard, 2007.

[7] W.W. Yu, C.S. Davis, Cold-formed steel members with perforated elements, Journal of the Structural Division, 99 (1973) 2061-2077.

[8] K.S. Sivakumaran, K.M. Zielonka, Web crippling strength of thin-walled steel members with web opening, Thin-Walled Structures, 8 (1989) 295-319.

[9] F. Zhou, B. Young, Web crippling of aluminium tubes with perforated webs, Engineering Structures, 32 (2010) 1397-1410.

[10] P. Natario, N. Silvestre, D. Camotim, Computational modelling of flange crushing in cold-formed steel sections, Thin-Walled Structures, 84 (2014) 393-405.

[11] P. Keerthan, M. Mahendran, E. Steau, Experimental study of web crippling behaviour of hollow flange channel beams under two flange load cases, Thin-Walled Structures, 85 (2014) 207-219.

[12] Y. Chen, XX. Chen, CY. Wang, Experimental and finite element analysis research on cold-formed steel lipped channel beams under web crippling, Thin-walled Structures, 87 (2015) 41-52.

[13] Y. Chen, XX. Chen, CY. Wang, Aluminum tubular sections subjected to web crippling, Thin-Walled Structures, 90 (2015) 49-60.

[14] Y. Lian, A. Uzzaman, J.B.P. Lim, G. Abdelal, D. Nash, B. Young, Effect of web holes on web crippling strength of cold-formed steel channel sections under end-one-

flange loading condition - Part I I: Parametric study and proposed design equations. Submitted to Thin-walled Structures.

[15] ABAQUS Analysis User's Manual-Version 6.13-1. ABAQUS Inc., USA, 2013.

[16] EN, 10002-1: 2001. Tensile testing of metallic materials. Method of test at ambient temperature, British Standards Institution, 2001.

[17] J.B.P. Lim, D.A. Nethercot, Finite element idealisation of a cold-formed steel portal frame, Journal of structural engineering, 130 (2004) 78-94.

[18] J.B.P. Lim, D.A. Nethercot, Stiffness prediction for bolted moment-connections between cold-formed steel members, Journal of constructional steel research, 60 (2004) 85-107.

Table 1   Measured specimen dimensions and experimental ultimate loads for flanges unfastened case

Specimen	Web	Flange	Lip	Thickness	Fillet	Holes		Length	Experiment result full pair	Exp. load per Web
	d	b_f	b_l	t	r_i	a_{LHS}	a_{RHS}	L	P_{EXP}	P_{EXP}
	(mm)	(mm)	(mm)	(mm)	(mm)	(mm)	(mm)	(mm)	(kN)	(kN)
142x60x13-t1.3-N100-A0-FR-T1	142.70	59.79	13.23	1.23	4.80	-	-	720.0	19.10	4.78
142x60x13-t1.3-N100-A0-FR-T2	142.17	59.98	13.18	1.23	4.80	-	-	720.0	19.22	4.81
142x60x13-t1.3-N100-A0-FR-T3	142.40	60.04	13.00	1.23	4.80	-	-	720.0	19.03	4.76
142x60x13-t1.3-N100-A0.4-FR-T1	142.27	60.02	13.11	1.23	4.80	55.30	55.20	720.0	18.11	4.53
142x60x13-t1.3-N100-A0.4-FR-T2	142.16	59.99	36.57	1.23	4.80	55.10	55.20	720.0	18.14	4.54
142x60x13-t1.3-N100-A0.4-FR-T3	142.16	59.98	13.18	1.23	4.80	55.15	55.20	720.0	18.32	4.58
142x60x13-t1.3-N100-MA0.4-FR-T1	141.85	60.08	13.13	1.23	4.80	55.02	55.21	720.0	14.52	3.63
142x60x13-t1.3-N100-MA0.4-FR-T2	142.13	60.05	13.13	1.23	4.80	55.53	55.35	720.0	15.65	3.91
142x60x13-t1.3-N100-MA0.4-FR-T3	142.19	60.07	13.13	1.23	4.80	55.56	55.09	720.0	15.32	3.83
142x60x13-t1.3-N120-A0-FR	142.09	60.07	13.34	1.25	4.80	-	-	760.0	21.64	5.41
142x60x13-t1.3-N120-A0.4-FR	142.22	60.03	13.11	1.23	4.80	55.16	55.17	760.0	18.66	4.66
142x60x13-t1.3-N120-MA0.4-FR	142.27	60.00	13.26	1.25	4.80	55.25	55.28	760.0	16.89	4.22
142x60x13-t1.3-N150-A0-FR	142.15	60.06	13.27	1.24	4.80	-	-	820.0	22.23	5.56
142x60x13-t1.3-N150-A0.4-FR	142.17	60.00	13.16	1.23	4.80	55.15	55.07	820.0	19.99	5.00
142x60x13-t1.3-N150-MA0.4-FR	142.30	60.01	13.12	1.24	4.80	55.15	55.20	820.0	18.37	4.59
202x65x15-t1.4-N100-A0-FR	201.99	65.36	14.84	1.35	5.00	-	-	900.0	13.72	3.43
202x65x15-t1.4-N100-A0.4-FR	202.02	65.04	15.01	1.35	5.00	79.35	79.34	900.0	13.72	3.43
202x65x15-t1.4-N100-MA0.4-FR	202.07	65.16	14.98	1.35	5.00	79.34	79.37	900.0	12.29	3.07
202x65x15-t1.4-N120-A0-FR	202.07	65.37	14.85	1.35	5.00	-	-	940.0	18.40	4.60
202x65x15-t1.4-N120-A0.4-FR	202.04	65.20	14.90	1.35	5.00	79.38	79.33	940.7	17.65	4.41
202x65x15-t1.4-N120-A0.6-FR	202.10	65.49	14.43	1.35	5.00	99.30	99.48	940.0	15.36	3.84
202x65x15-t1.4-N120-MA0.4-FR	202.02	65.42	14.75	1.35	5.00	79.32	79.35	940.0	15.57	3.89
202x65x15-t1.4-N120-MA0.6-FR	202.06	65.25	14.52	1.35	5.00	99.41	99.11	940.0	15.36	3.54
202x65x15-t1.4-N150-A0-FR	202.13	65.40	14.72	1.35	5.00	-	-	1000.0	19.85	4.96
202x65x15-t1.4-N150-A0.4-FR	202.05	65.22	14.87	1.35	5.00	79.40	79.40	999.0	17.48	4.37

202x65x15-t1.4-N150-A0.6-FR	201.89	65.38	14.36	1.35	5.00	99.37	99.56	1000.0	17.48	4.44
202x65x15-t1.4-N150-MA0.4-FR	202.07	65.28	14.95	1.35	5.00	79.36	79.34	1000.0	16.40	4.10
202x65x15-t1.4-N150-MA0.6-FR	202.41	65.26	14.31	1.35	5.00	99.59	99.44	1000.0	15.38	3.85
302x90x18-t2.0-N100-A0-FR	303.42	88.20	18.56	1.90	5.00	-	-	1199.0	31.69	7.92
302x90x18-t2.0-N100-A0.6-FR	303.04	88.15	18.67	1.90	5.00	179.09	179.04	1200.0	27.19	6.80
302x90x18-t2.0-N100-MA0.2-FR	303.02	88.05	18.69	1.90	5.00	60.00	60.02	1199.0	31.99	8.00
302x90x18-t2.0-N120-A0-FR	302.35	89.08	18.61	1.90	5.00	-	-	1238.8	34.63	8.66
302x90x18-t2.0-N120-A0.6-FR	302.82	89.10	18.20	1.90	5.00	178.37	178.92	1240.2	30.58	7.64
302x90x18-t2.0-N120-MA0.3-FR	303.63	89.30	18.62	1.90	5.00	89.54	89.61	1239.0	34.49	8.62
302x90x18-t2.0-N150-A0-FR	303.37	88.86	18.45	1.90	5.00	-	-	1299.9	35.23	8.81
302x90x18-t2.0-N150-A0.6-FR	303.18	89.37	18.40	1.90	5.00	178.85	178.91	1299.8	31.67	7.92
302x90x18-t2.0-N150-MA0.4-FR	303.47	89.73	18.38	1.90	5.00	119.38	119.17	1300.2	33.21	8.30

Table 2   Measured specimen dimensions and experimental ultimate loads for flanges fastened case

Specimen	Web	Flange	Lip	Thickness	Fillet	Holes		Length	Experiment Result full pair	Exp. load per Web
	d	b_f	b_l	t	r_i	a_{LHS}	a_{RHS}	L	P_{EXP}	P_{EXP}
	(mm)	(mm)	(mm)	(mm)	(mm)	(mm)	(mm)	(mm)	(kN)	(kN)
142x60x13-t1.3-N100-A0-FX-T1	142.13	60.06	13.17	1.27	4.80	-	-	720.0	28.30	7.07
142x60x13-t1.3-N100-A0-FX-T2	142.20	60.09	13.09	1.27	4.80	-	-	720.0	27.18	6.80
142x60x13-t1.3-N100-A0-FX-T3	142.18	60.01	13.10	1.27	4.80	-	-	720.0	28.17	7.04
142x60x13-t1.3-N100-A0.4-FX-T1	142.06	60.02	13.06	1.27	4.80	55.27	55.26	720.0	27.15	6.79
142x60x13-t1.3-N100-A0.4-FX-T2	142.11	60.07	13.12	1.27	4.80	55.26	55.28	720.0	26.71	6.68
142x60x13-t1.3-N100-A0.4-FX-T3	142.16	60.02	13.20	1.27	4.80	55.28	55.20	720.0	26.32	6.58
142x60x13-t1.3-N100-MA0.4-FX-T1	142.18	60.11	13.22	1.25	4.80	55.14	55.19	720.0	22.73	5.68
142x60x13-t1.3-N100-MA0.4-FX-T2	142.31	60.10	13.13	1.25	4.80	55.22	55.29	720.0	22.53	5.63
142x60x13-t1.3-N100-MA0.4-FX-T3	142.38	60.19	13.08	1.25	4.80	55.27	55.25	720.0	22.79	5.70
142x60x13-t1.3-N120-A0-FX	142.15	60.09	13.06	1.24	4.80	-	-	760.0	29.32	7.33
142x60x13-t1.3-N120-A0.4-FX	142.17	60.13	13.11	1.24	4.80	55.30	55.28	760.0	28.31	7.08
142x60x13-t1.3-N120-MA0.4-FX	142.21	59.96	13.13	1.24	4.80	55.20	55.18	760.0	24.52	6.13
142x60x13-t1.3-N150-A0-FX	142.27	59.99	13.14	1.23	4.80	-	-	820.0	31.89	7.97
142x60x13-t1.3-N150-A0.4-FX	142.26	60.09	13.21	1.23	4.80	55.25	55.25	820.0	28.96	7.24
142x60x13-t1.3-N150-MA0.4-FX	142.20	60.09	13.20	1.23	4.80	55.27	55.25	820.0	27.77	6.94
202x65x15-t1.4-N100-A0-FX	202.01	65.57	14.51	1.35	5.00	-	-	900.0	26.11	6.53
202x65x15-t1.4-N100-A0.4-FX	202.01	65.22	14.86	1.35	5.00	79.32	79.35	899.0	25.55	6.39
202x65x15-t1.4-N100-MA0.4-FX	202.00	65.27	14.77	1.35	5.00	79.33	79.33	899.0	21.54	5.39
202x65x15-t1.4-N120-A0-FX	202.02	65.39	14.71	1.35	5.00	-	-	939.0	28.43	7.11
202x65x15-t1.4-N120-A0.4-FX	202.00	65.43	14.84	1.35	5.00	79.31	79.36	939.3	26.43	6.61
202x65x15-t1.4-N120-A0.6-FX	201.60	65.46	14.24	1.33	5.00	99.53	99.46	940.0	23.93	5.98
202x65x15-t1.4-N120-MA0.4-FX	202.01	65.43	14.71	1.33	5.00	79.33	79.34	940.0	22.13	5.53
202x65x15-t1.4-N120-MA0.6-FX	201.46	65.38	14.54	1.40	5.00	99.38	99.52	940.0	21.14	5.28
202x65x15-t1.4-N150-A0-FX	202.01	65.45	14.75	1.35	5.00	-	-	999.0	30.90	7.73
202x65x15-t1.4-N150-A0.4-FX	202.03	65.18	14.77	1.33	5.00	79.33	79.40	999.0	28.48	7.12
202x65x15-t1.4-N150-A0.6-FX	202.43	65.42	14.36	1.34	5.00	99.52	99.61	1000.0	27.19	6.80

18

202x65x15-t1.4-N150-MA0.4-FX	202.08	65.22	14.68	1.33	5.00	79.34	79.31	999.0	25.00	6.25
202x65x15-t1.4-N150-MA0.6-FX	202.41	65.18	14.30	1.40	5.00	99.48	99.96	1000.0	23.76	5.94
302x90x18-t2.0-N100-A0-FX	302.91	88.61	18.66	1.76	5.00	-	-	1199.7	44.29	11.07
302x90x18-t2.0-N100-A0.6-FX	303.03	88.37	18.51	1.80	5.00	178.78	178.74	1200.2	40.38	10.09
302x90x18-t2.0-N100-MA0.2-FX	303.33	88.33	18.67	1.75	5.00	59.87	59.70	1200.1	40.91	10.23
302x90x18-t2.0-N120-A0-FX	303.36	89.06	18.79	1.80	5.00	-	-	1242.0	49.23	12.31
302x90x18-t2.0-N120-A0.6-FX	303.08	88.66	18.35	1.80	5.00	178.77	178.75	1241.0	41.75	10.44
302x90x18-t2.0-N120-MA0.3-FX	303.08	88.26	18.49	1.80	5.00	89.86	89.92	1239.0	45.10	11.27
302x90x18-t2.0-N150-A0-FX	303.36	88.65	18.63	1.75	5.00	-	-	1298.0	50.32	12.58
302x90x18-t2.0-N150-A0.6-FX	303.62	88.50	18.58	1.75	5.00	178.92	178.62	1302.3	43.13	10.78
302x90x18-t2.0-N150-MA0.4-FX	303.52	88.58	18.43	1.80	5.00	119.22	119.43	1298.7	43.69	10.92

Table 3   Measured material properties of specimens

| Section	$\sigma_{0.2}$ (MPa)	σ_u (MPa)
142 x 60 x 13 x 1.3	457	496
202 x 65 x 15 x 1.4	464	566
302 x 88 x 18 x 2.0	479	575

Table 4   Comparison of web crippling strength predicted from finite element analysis with experiment results for flanges unfastened case

Specimen	Web slenderness	Hole diameter ratio	Exp. load per web	Web crippling strength per web predicted from FEA	Comparison
	(h/t)	(a/h)	P_{EXP} (kN)	P_{FEA} (kN)	P_{EXP} / P_{FEA}
142x60x13-t1.3-N100-A0-FR-T1	114.01	-	4.78	4.77	1.00
142x60x13-t1.3-N100-A0-FR-T2	113.58	-	4.81	4.77	1.01
142x60x13-t1.3-N100-A0-FR-T3	113.77	-	4.76	4.77	1.00
142x60x13-t1.3-N100-A0.4-FR-T1	113.66	0.40	4.53	4.48	1.01
142x60x13-t1.3-N100-A0.4-FR-T2	113.57	0.39	4.54	4.48	1.01
142x60x13-t1.3-N100-A0.4-FR-T3	113.58	0.39	4.58	4.48	1.02
142x60x13-t1.3-N100-MA0.4-FR-T1	113.33	0.39	3.63	3.96	0.92
142x60x13-t1.3-N100-MA0.4-FR-T2	113.55	0.40	3.91	3.96	0.99
142x60x13-t1.3-N100-MA0.4-FR-T3	113.60	0.40	3.83	3.96	0.97
142x60x13-t1.3-N120-A0-FR	111.67	-	5.41	5.33	1.02
142x60x13-t1.3-N120-A0.4-FR	113.62	0.39	4.66	4.88	0.96
142x60x13-t1.3-N120-MA0.4-FR	111.81	0.40	4.22	4.48	0.94
142x60x13-t1.3-N150-A0-FR	112.64	-	5.56	5.64	0.99
142x60x13-t1.3-N150-A0.4-FR	113.59	0.39	5.00	5.18	0.96
142x60x13-t1.3-N150-MA0.4-FR	112.76	0.39	4.59	4.68	0.98
202x65x15-t1.4-N100-A0-FR	147.62	-	3.43	4.52	0.76
202x65x15-t1.4-N100-A0.4-FR	147.65	0.40	3.43	4.19	0.82
202x65x15-t1.4-N100-MA0.4-FR	147.68	0.40	3.07	3.57	0.86
202x65x15-t1.4-N120-A0-FR	147.68	-	4.60	4.62	1.00
202x65x15-t1.4-N120-A0.4-FR	147.66	0.40	4.41	4.41	1.00
202x65x15-t1.4-N120-A0.6-FR	147.70	0.50	3.84	3.93	0.98
202x65x15-t1.4-N120-MA0.4-FR	147.65	0.40	3.89	3.98	0.98
202x65x15-t1.4-N120-MA0.6-FR	147.67	0.50	3.54	3.48	1.02
202x65x15-t1.4-N150-A0-FR	147.72	-	4.96	5.02	0.99
202x65x15-t1.4-N150-A0.4-FR	147.67	0.40	4.37	4.67	0.94
202x65x15-t1.4-N150-A0.6-FR	147.55	0.50	4.44	4.44	1.00

202x65x15-t1.4-N150-MA0.4-FR	147.68	0.40	4.10	4.24	0.97
202x65x15-t1.4-N150-MA0.6-FR	147.93	0.50	3.85	3.74	1.03
302x90x18-t2.0-N100-A0-FR	157.69	-	7.92	8.36	0.95
302x90x18-t2.0-N100-A0.6-FR	157.49	0.60	6.80	6.89	0.99
302x90x18-t2.0-N100-MA0.2-FR	157.48	0.20	8.00	8.07	0.99
302x90x18-t2.0-N120-A0-FR	157.13	-	8.66	8.61	1.01
302x90x18-t2.0-N120-A0.6-FR	157.38	0.60	7.64	7.62	1.00
302x90x18-t2.0-N120-MA0.3-FR	157.80	0.30	8.62	8.64	1.00
302x90x18-t2.0-N150-A0-FR	157.67	-	8.81	9.17	0.96
302x90x18-t2.0-N150-A0.6-FR	157.57	0.60	7.92	7.96	0.99
302x90x18-t2.0-N150-MA0.4-FR	157.72	0.40	8.30	8.30	1.00
Mean					0.97
COV					0.057

Table 5   Comparison of web crippling strength predicted from finite element analysis with experiment results for flanges fastened case

Specimen	Web slenderness	Hole diameter ratio	Exp. load per web	Web crippling strength per web predicted from FEA	Comparison
	(h/t)	(a/h)	P_{EXP} (kN)	P_{FEA} (kN)	P_{EXP} / P_{FEA}
142x60x13-t1.3-N100-A0-FX-T1	109.92	0.00	7.07	7.06	1.00
142x60x13-t1.3-N100-A0-FX-T2	109.97	0.00	6.80	7.06	0.96
142x60x13-t1.3-N100-A0-FX-T3	109.95	0.00	7.04	7.06	1.00
142x60x13-t1.3-N100-A0.4-FX-T1	109.86	0.40	6.79	6.80	1.00
142x60x13-t1.3-N100-A0.4-FX-T2	109.90	0.40	6.68	6.80	0.98
142x60x13-t1.3-N100-A0.4-FX-T3	109.94	0.40	6.58	6.80	0.97
142x60x13-t1.3-N100-MA0.4-FX-T1	111.75	0.39	5.68	5.80	0.98
142x60x13-t1.3-N100-MA0.4-FX-T2	111.85	0.39	5.63	5.80	0.97
142x60x13-t1.3-N100-MA0.4-FX-T3	111.90	0.40	5.70	5.80	0.98
142x60x13-t1.3-N120-A0-FX	112.64	0.00	7.33	7.28	1.01
142x60x13-t1.3-N120-A0.4-FX	112.65	0.40	7.08	7.01	1.01
142x60x13-t1.3-N120-MA0.4-FX	112.68	0.40	6.13	6.24	0.98
142x60x13-t1.3-N150-A0-FX	113.67	0.00	7.97	7.95	1.00
142x60x13-t1.3-N150-A0.4-FX	113.66	0.40	7.24	7.65	0.95
142x60x13-t1.3-N150-MA0.4-FX	113.61	0.40	6.94	6.96	1.00
202x65x15-t1.4-N100-A0-FX	147.63	0.00	6.53	6.61	0.99
202x65x15-t1.4-N100-A0.4-FX	147.64	0.40	6.39	6.35	1.01
202x65x15-t1.4-N100-MA0.4-FX	147.63	0.40	5.39	5.45	0.99
202x65x15-t1.4-N120-A0-FX	147.64	0.00	7.11	7.04	1.01
202x65x15-t1.4-N120-A0.4-FX	147.63	0.40	6.61	6.77	0.98
202x65x15-t1.4-N120-A0.6-FX	149.58	0.50	5.98	6.06	0.99
202x65x15-t1.4-N120-MA0.4-FX	149.88	0.40	5.53	5.74	0.96
202x65x15-t1.4-N120-MA0.6-FX	141.90	0.50	5.28	4.85	1.09
202x65x15-t1.4-N150-A0-FX	147.64	0.00	7.73	7.78	0.99

202x65x15-t1.4-N150-A0.4-FX	149.90	0.40	7.12	7.24	0.98
202x65x15-t1.4-N150-A0.6-FX	149.07	0.50	6.80	6.78	1.00
202x65x15-t1.4-N150-MA0.4-FX	149.94	0.40	6.25	6.42	0.97
202x65x15-t1.4-N150-MA0.6-FX	142.58	0.50	5.94	5.94	1.00
302x90x18-t2.0-N100-A0-FX	170.11	0.00	11.07	11.16	0.99
302x90x18-t2.0-N100-A0.6-FX	166.35	0.60	10.09	9.74	1.04
302x90x18-t2.0-N100-MA0.2-FX	171.33	0.20	10.23	10.67	0.96
302x90x18-t2.0-N120-A0-FX	166.54	0.00	12.31	12.42	0.99
302x90x18-t2.0-N120-A0.6-FX	166.38	0.60	10.44	10.46	1.00
302x90x18-t2.0-N120-MA0.3-FX	166.38	0.30	11.27	11.14	1.01
302x90x18-t2.0-N150-A0-FX	171.35	0.00	12.58	13.04	0.96
302x90x18-t2.0-N150-A0.6-FX	171.50	0.60	10.78	10.76	1.00
302x90x18-t2.0-N150-MA0.4-FX	166.62	0.40	10.92	10.90	1.00
Mean					0.99
COV					0.025
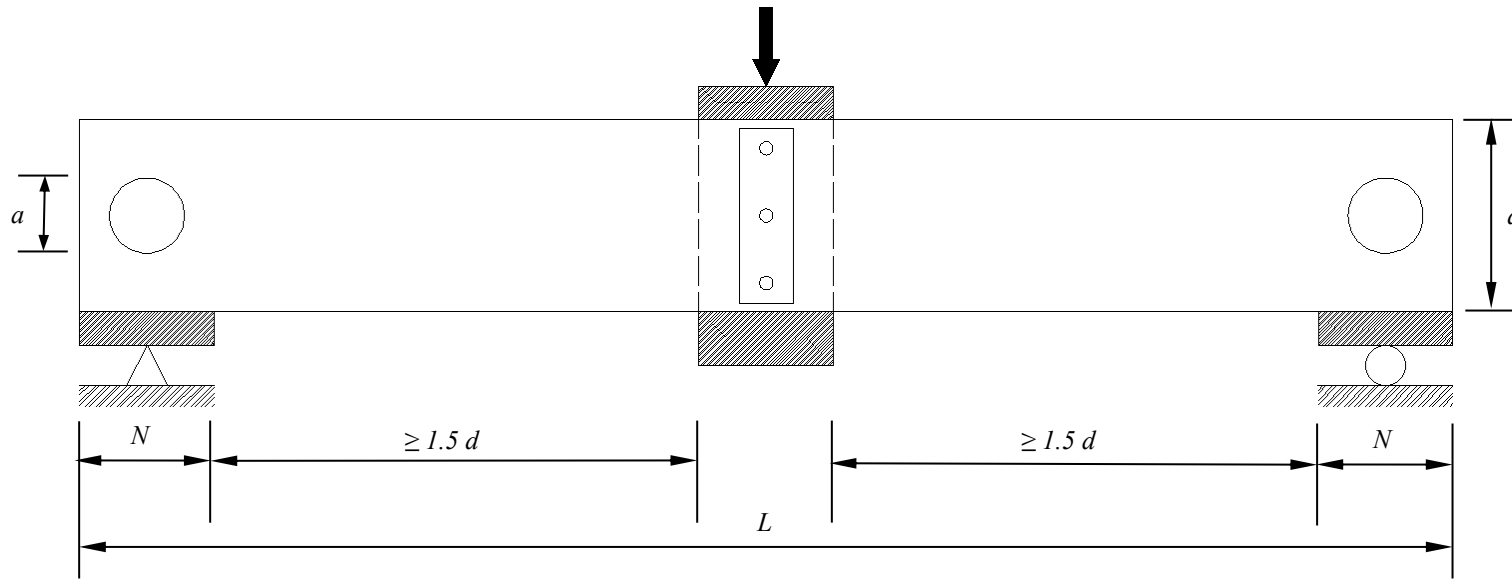
(a) With holes centred above bearing plate
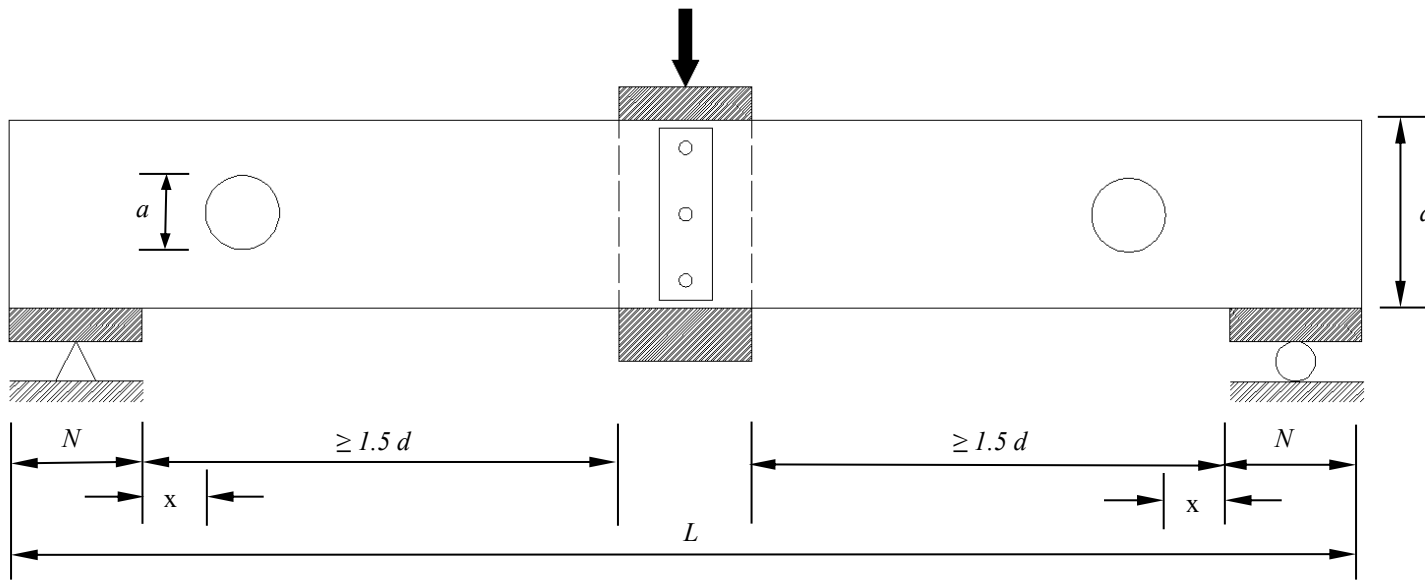
(b) With holes offset from bearing plate

Fig.1   End-one-flange loading condition
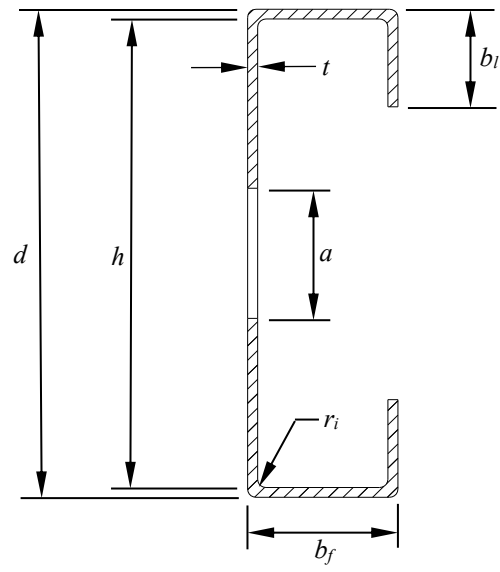
Fig.2   Definition of symbols
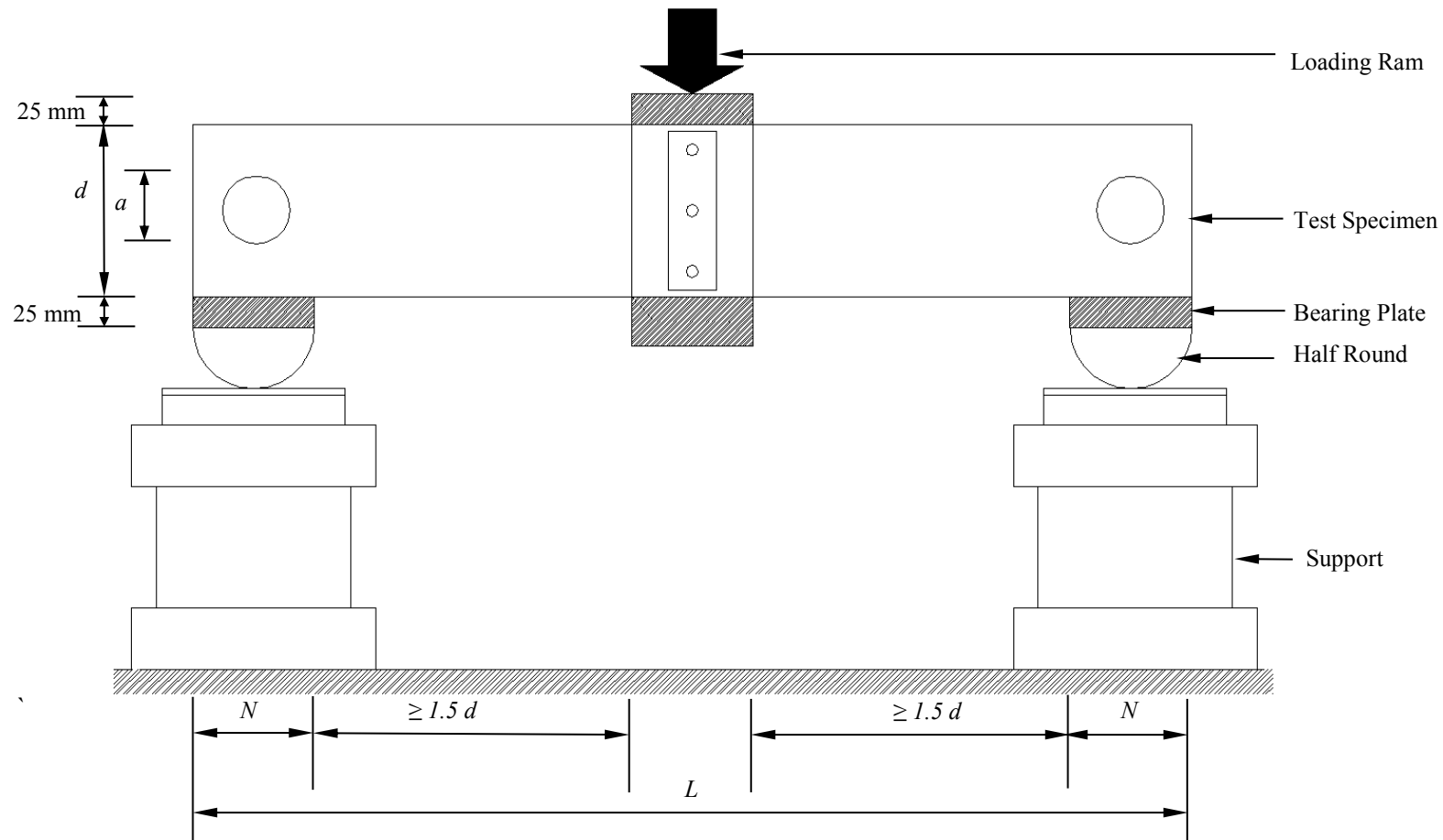
(a) Front view of with holes centred above bearing plate
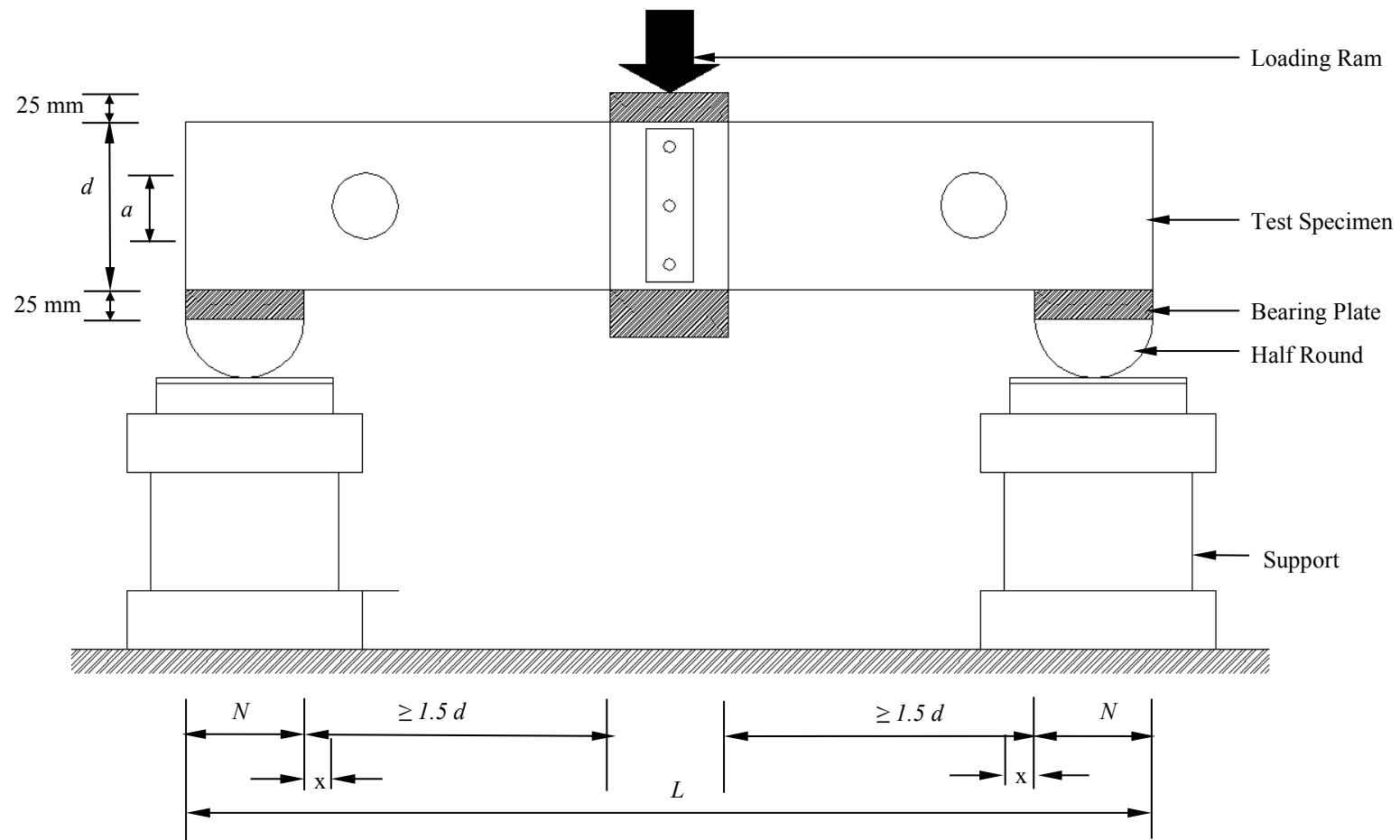
(b) Front view of with a horizontal clear distance to near edge of bearing plates

Loading Ram

Load Transfer Plate

Load Transfer Block

Test Specimen

Bolt at Loading Point

Bolts

Bearing Plate

Half Round

Teflon Pad

Load Transfer Plate

Support

(c) End View (Unfastened flanges)

(d) End View (Fastened flanges)
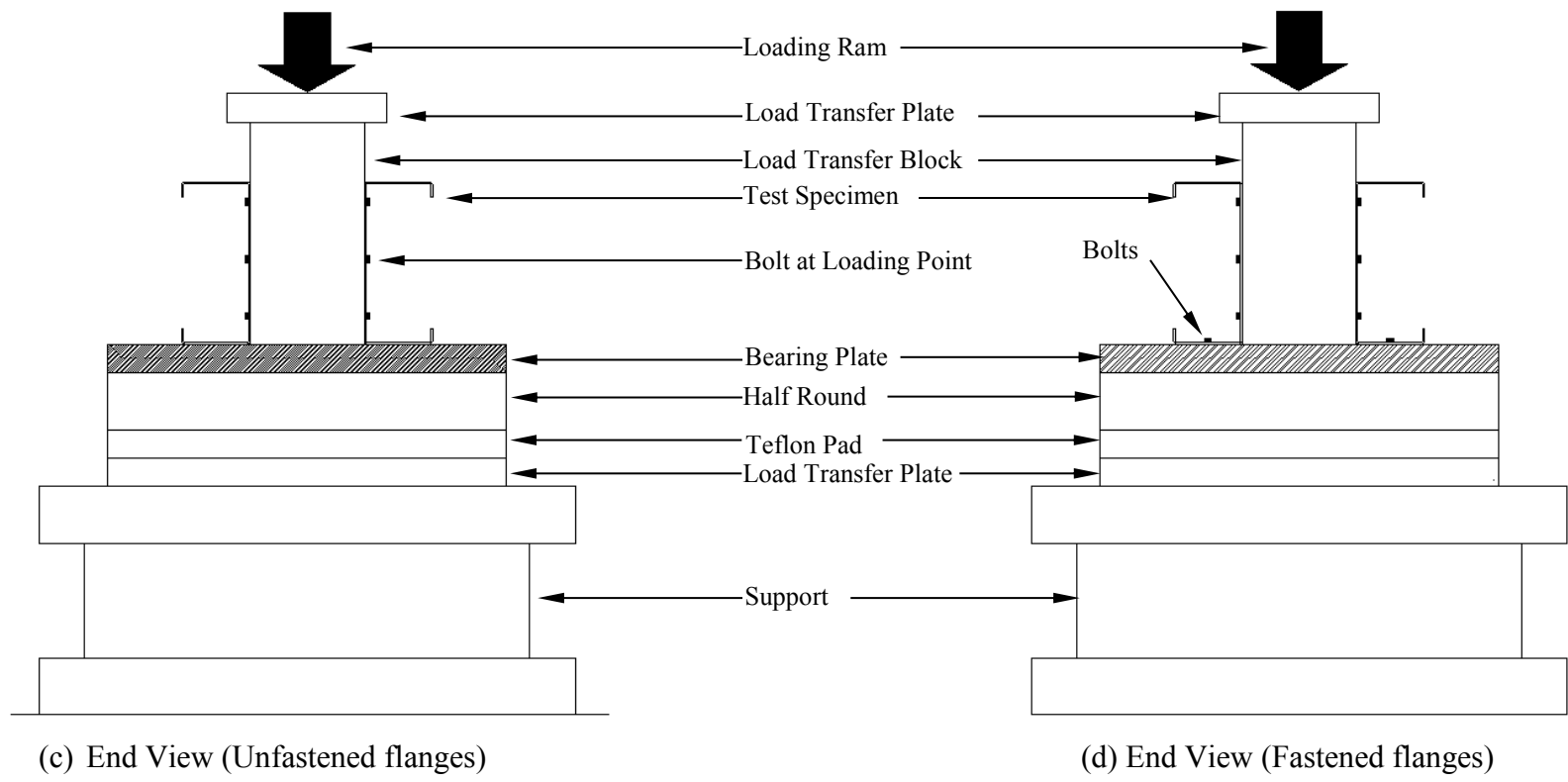
Fig.3   Schematic view of test set-up
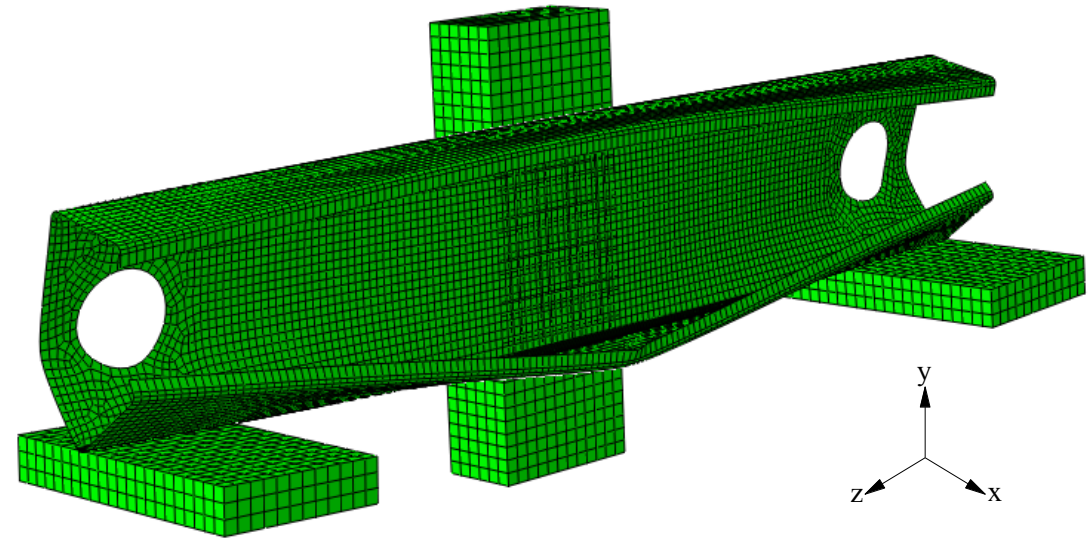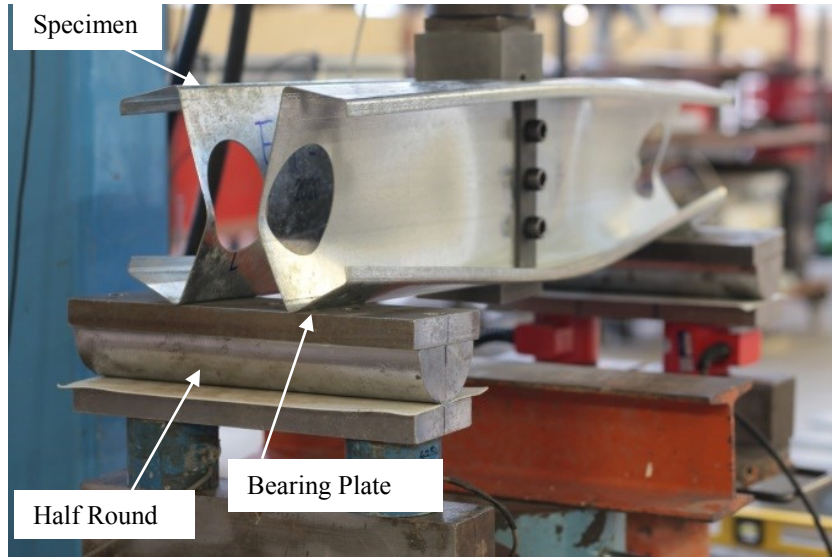
(a) Experimental   (b) FEA

Fig.4   Comparison of experiment and finite element analysis for centred hole where flanges unfastened to bearing plates
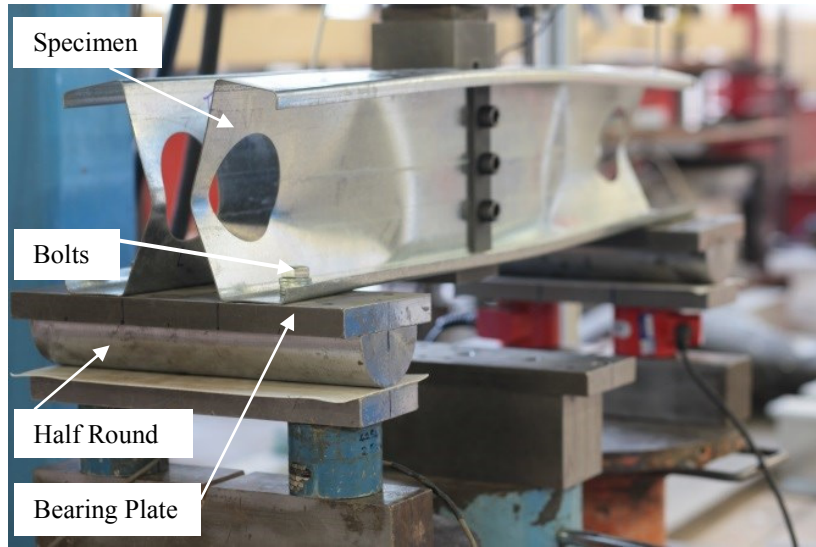
(b) FEA

Fig.5   Comparison of experiment and finite element analysis for centred hole where flanges fastened to bearing plates

31
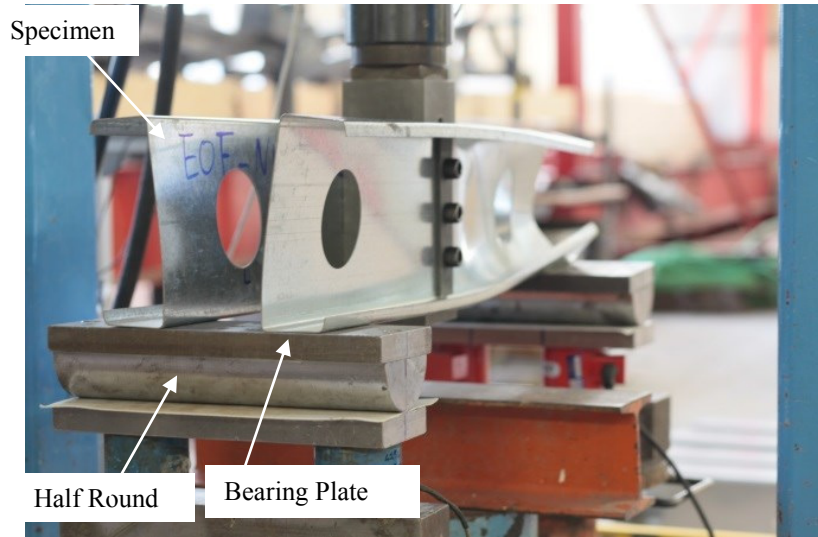
(a) Experimental   (b) FEA

Fig.6   Comparison of experiment and finite element analysis for offset hole where flanges unfastened to bearing plates
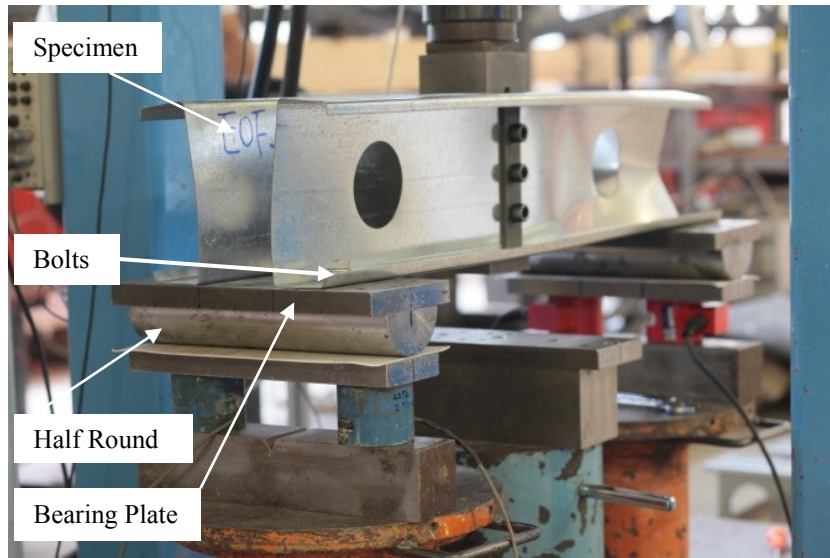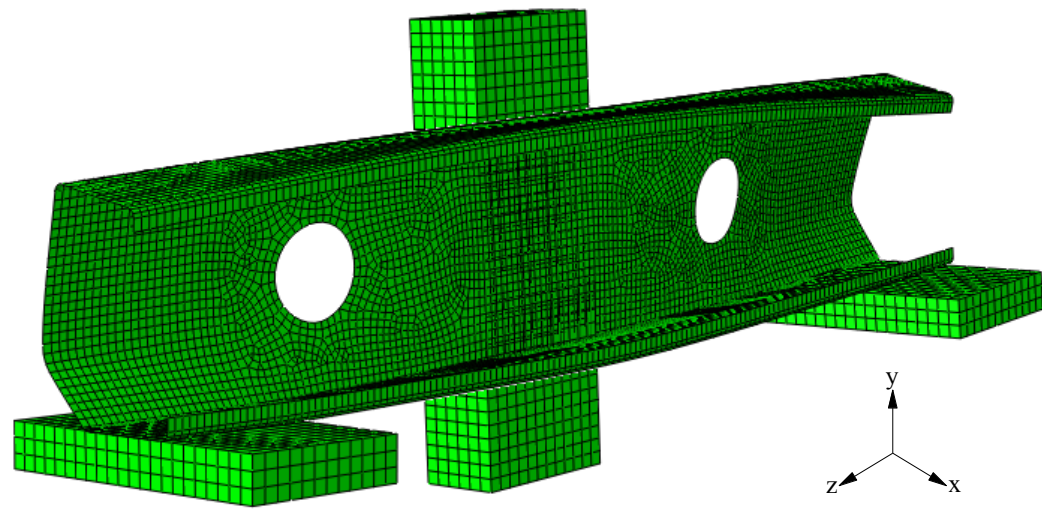
<table>
<tr><td>(a) Experimental</td><td>(b) FEA</td></tr>
</table>

Fig.7   Comparison of experiment and finite element analysis for offset hole where flanges fastened to bearing plates
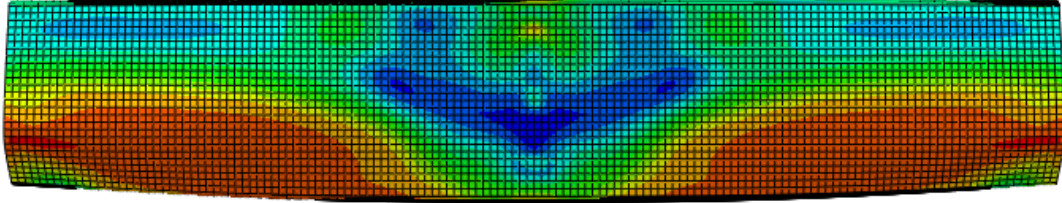
(a) Comparison of deformation shape for without holes
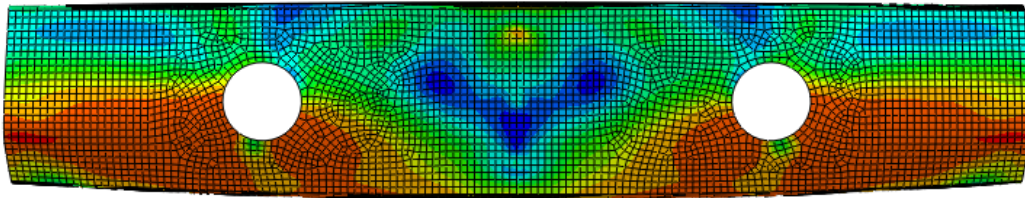
(b) Comparison of deformation shape for offset holes
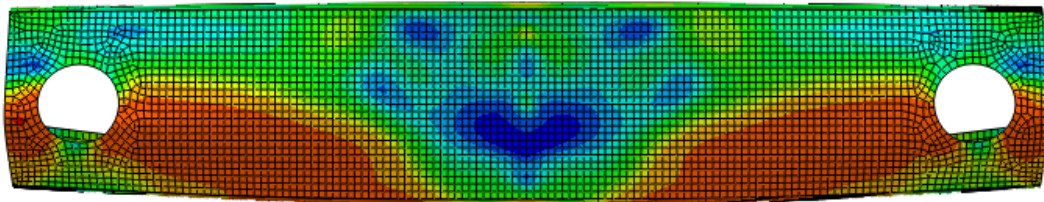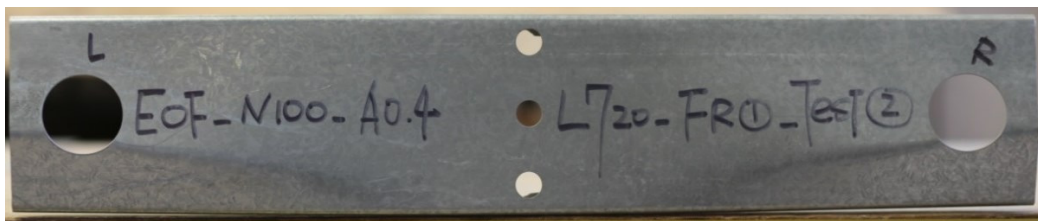
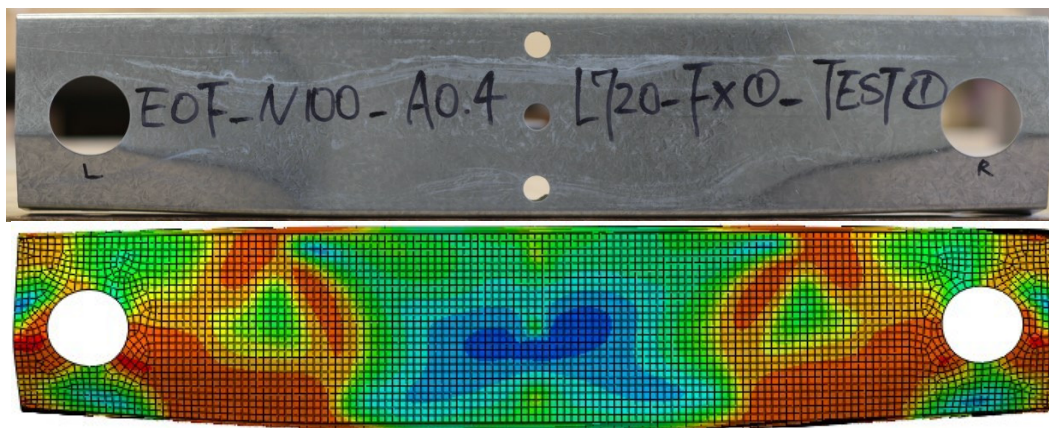(c) Comparison of deformation shape for centred holes

Fig.8　　Comparison of the deformation shape for the flanges unfastened to the bearing plates
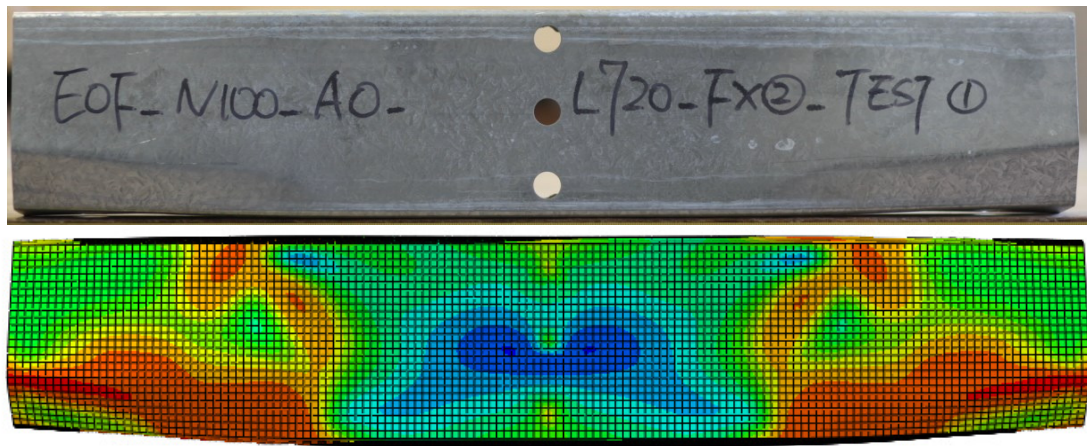
(a) Comparison of deformation shape for without holes
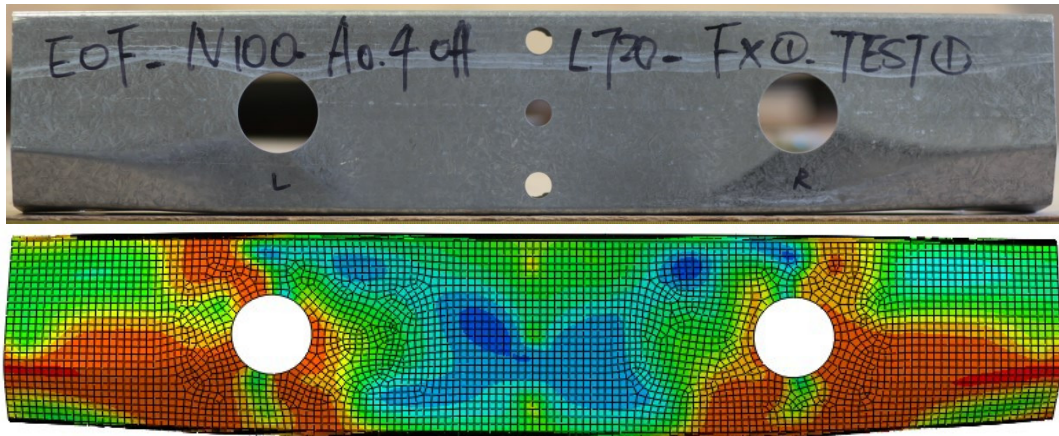
(b) Comparison of deformation shape for offset holes

(c) Comparison of deformation shape for centred holes

Fig.9   Comparison of the deformation shape for the flanges fastened to the bearing plates
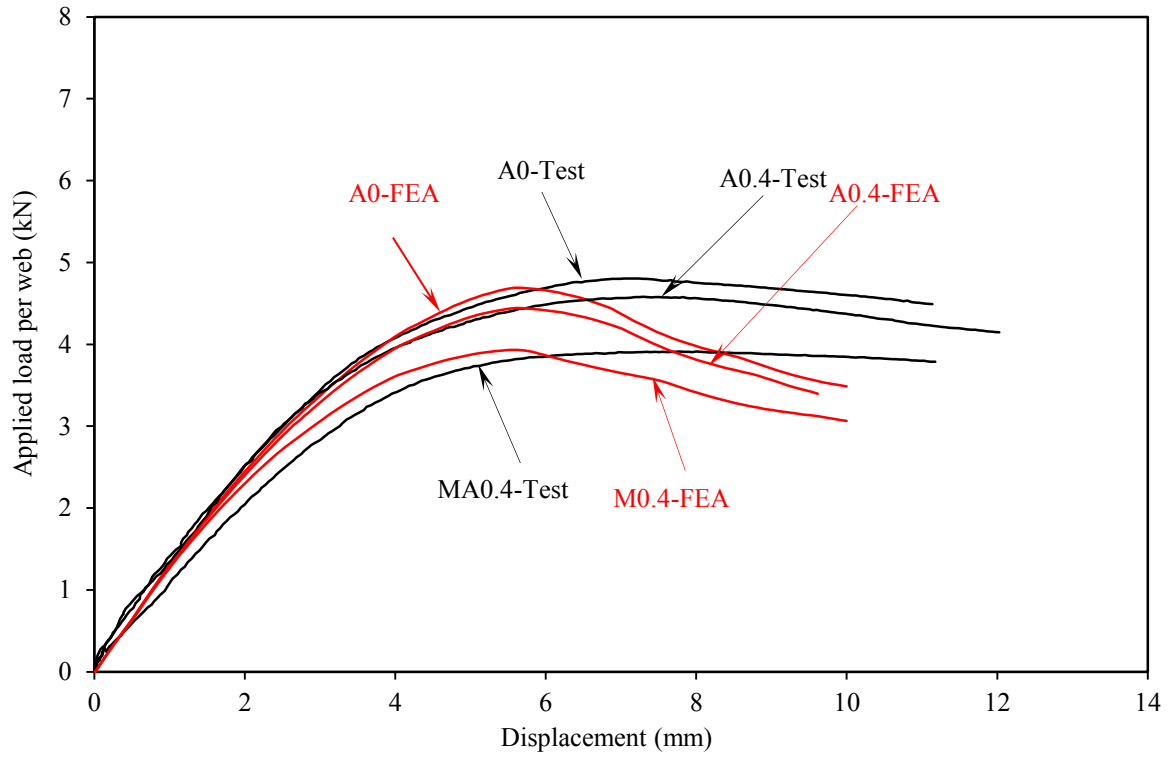
Fig.10   Comparison of web deformation curves for specimen 142×60×13-t1.3-N100-FR
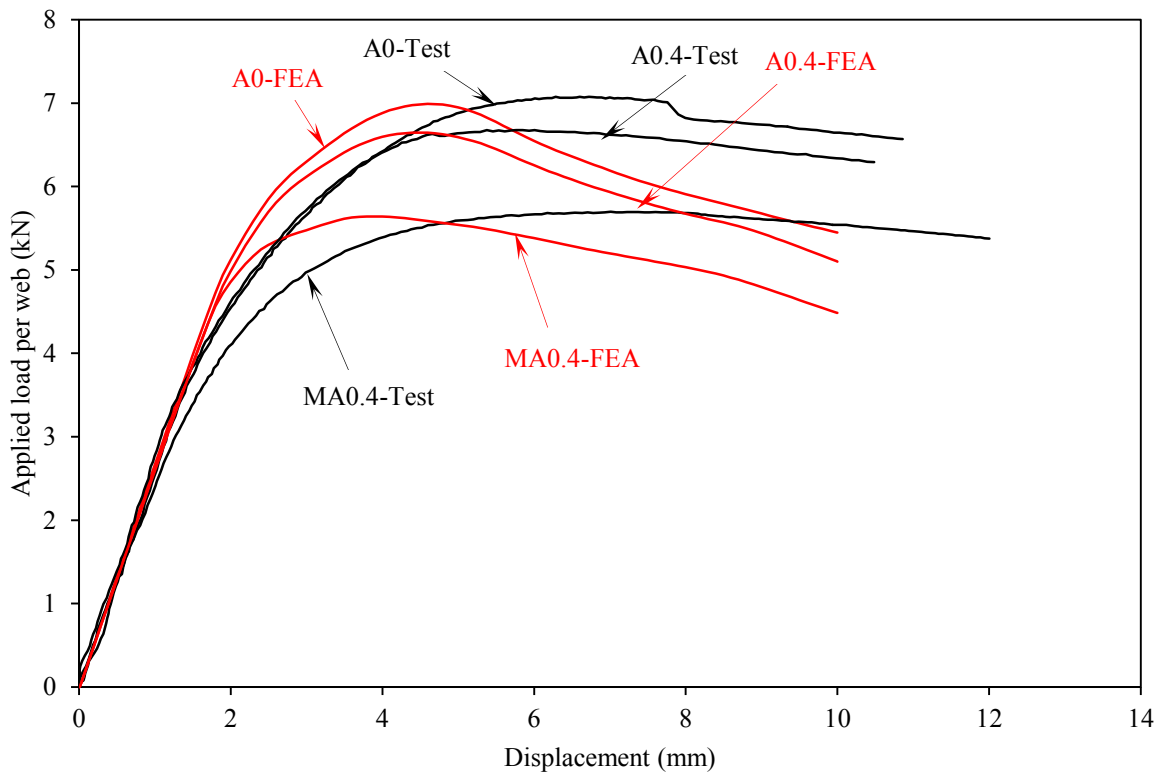

Fig.11   Comparison of web deformation curves for specimen 142×60×13-t1.3-N100-FX